Evaluation of variation of gas flow rate during pyrolysis of negative photo-resist derived carbon electrodes for electrochemical and surface optimization

Fabian Oswaldo Romero Soto A01337827
M-5052.1 Material Characterization

Introduction

In the last two decades, there has been development of biological and medical devices able of using and controlling fluids in micro/nanoscale. Controlling elements on these scales can offer many advantages such as: low sample volume, automation, portability, low cost and high throughput screening **(1)**. These kinds of platforms can be used to adapt multiple chemical and biological assays, specially in a rough and low-resources or Point of Care (PoC) environments. Microfluidic platforms such as Lab on a Chip (LoC) and Lab on a Disc (LoD) are examples of systems that integrate laboratory processes in a miniaturized presentation.

The electrochemical analysis is one of the applications that it can be integrated in the microfluidic platforms for analytical assays. This method is commonly used by the simple implementation to measure continuously a target molecule during a redox reaction. Molecules such as dopamine **(2)** and C-reactive protein (CRP) **(3)** have been targets to quantify the current generated during the reaction and decide a diagnosis. Other process that it can take approach by the electrical behavior of the target molecule is the separation by Dielectrophoresis (DEP). Martinez-Duarte et al. **(4)** implemented dielectrophoresis as an active filter (by the gradient of electrical fields) to separate yeast particles during a running lab on a Disc. The previous examples are possible to implement because of the development of microelectrodes for the electrical interaction on this scale.

Carbon is the most common material for electrodes fabrication due to the different properties that it can offer such as: wide electrochemical window, chemical inertness, low fabrication costs and biocompatibility **(5–7)**. There are variations of carbon as graphite and glassy carbon, where the last one is commonly used for microelectromechanical systems (MEMS) purposes. It is possible to use a derived glassy carbon to generate micropatterns from hundreds of micrometers to tens of nanometers by using SU-8, an epoxy-based negative photoresist **(8)**. The versatility to acquire a variety of patterns and structures while tuning its physical and electrical properties, photoresists are common for C-MEMS fabrication.

The pyrolysis, or thermal degradation, consists of leading the formation of glassy-like carbon by retiring the rest of volatile materials by heating, as SU-8, during an inert atmosphere **(9)**. One of the first works related to the fabrication of microelectrodes by applying patterning photolithography and pyrolysis was Ranganathan et al. **(10)**. The process of pyrolysis can be divided mainly in two stages **(8)**: (a) pre-carbonization and (b) carbonization. In the pre-carbonization stage (T< 300 °C) the molecules of solvent and

unreacted monomer are eliminated from the polymeric precursor. The carbonization step can be divided in two sub-stages: (i) from 300 to 500 °C, oxygen and halogens are eliminated from the polymer leading to a loss of mass; (ii) from 500 to 1200 °C, hydrogen, oxygen and nitrogen atoms are eliminated, and the aromatic network is forced to become interconnected. This stage aids the creation of structure of the hybridization of C bonds on sp^2 (graphitic zone) and sp^3 (amorphous zone), relating the modification of properties such as permeability, density, hardness, Young´s modulus and conductivity **(5,8)**. In the **Figure 1** is shown the representation of each step done during the fabrication of carbon structures.

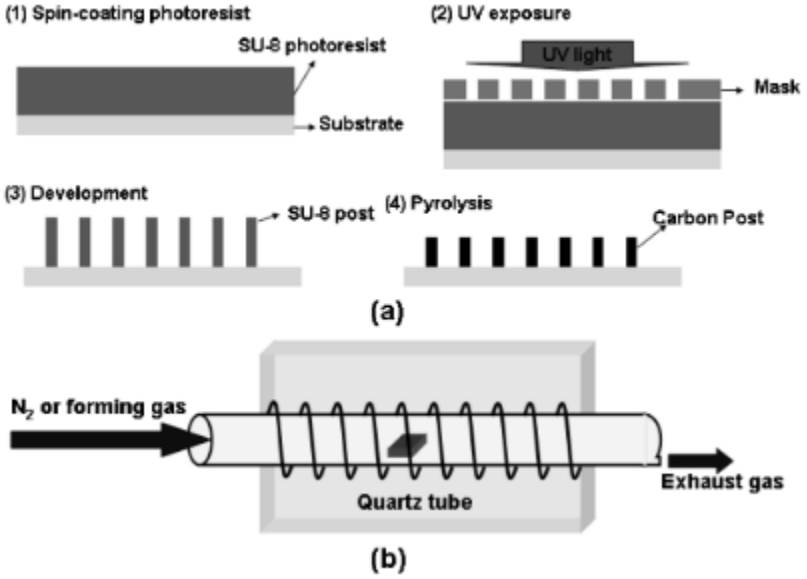

Figure 1. Fabrication steps for glassy carbon structures, including photolithography and pyrolysis **(11)**

Multiple works have focused on the optimization of parameters used during the pyrolysis such as heat ramp, dwell time in the carbonization and type of inert atmosphere **(5–7,12–15)**. However, there is not a study where it quantifies the differences that the change of flow rate in the gas supply for pyrolysis can generate in the electrochemical and surface properties in the sample. Considering that the gas supply aids to deliver the heat inside of the furnace, it is important consider that it could exist a temperature gradient inside of it depending of where the entrance of the gas supply and temperature sensor are localized. This heat transfer can affect the thermal homogeneity in the samples inside of the furnace, modifying the electrochemical properties of each sample. As well, the same substrates act as an obstacle for this supply, generating physical stress for them. Lyons et al. **(16)** has studied the differences that the shrinkage in the material can suffer depending if the gas used for the inert atmosphere is either hydrogen or nitrogen.

This work focuses to check how the variation of gas flow rate can affect the electrochemical and surface properties on electrodes from the same sample while maintaining repeatability and uniformity. We compare the electrodes obtained from

different flow rates by evaluating them with the electrochemical and surface properties. For this purpose, it will be employed characterization techniques to evaluate the morphological state of the electrodes (Scanning Electronic Microscope and Optical Microscope), chemical composition (Raman spectroscopy and X-ray Photoelectron Spectroscopy) as well as electrochemical behavior (Cyclic Voltammetry and Electrochemical Impedance Spectroscopy). These characterization techniques will provide both quantifiable and qualifiable data about the variation of electrical properties in GC electrodes by the difference of flow rate during the pyrolysis, either the position of the substrate or the physical position of the electrode through the Quartz tube.

Methodology

Materials

SU-8 2007 and SU-8 Developer were obtained from MicroChem Inc., MA, USA. Silicon wafers (diameter 100 mm, orientation (100), type p) used as substrate were provided by University Wafers, MA, USA. Potassium chloride (KCl), Potassium hexacyanoferrate (II) trihydrate ($C_6FeK_4N_6 \cdot 3H_2O$) and Potassium hexacyanoferrate (III) ($C_6FeK_3N_6$) were purchased from Sigma-Aldrich, MO, USA. The Ultra-pure nitrogen tank (99.99%) used during the pyrolysis was provided by AOC Mexico, COAH, Mexico.

Fabrication of electrodes

- Standard Photolithography

The silicon substrates are cleaned with acetone, isopropanol and deionized water and then put in plasma cleaner (Harrick Plasma, NY, USA) for 3 minutes prior to the spin-coating step. The SU-8 was spin-coated at 3500 RPM for 30 seconds to obtain thick layers of 7 µm. The samples were soft baked at 95 °C for 4 minutes on a hotplate, then was exposed to UV light through a contact mask (**Figure 2**). The post-exposure bake was carried on a hotplate at 95 °C for 2.5 minutes and then, the samples were immersed to developer for 7 minutes, with moderate agitation, to remove the unexposed polymer. Finally, the samples were hard baked on a hotplate at 200 °C for 1 hour.

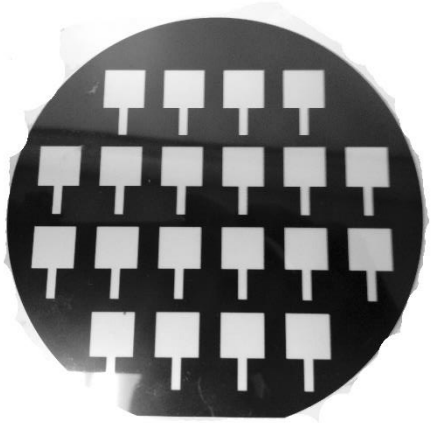

Figure 2. Mask design used for UV exposition during photolithography.

- Pyrolysis Process

Prior to the pyrolysis, the substrates with photoresist structures were cut to half vertically to cover along all the Quartz tube. The pyrolysis was done in an enclosed quartz tube furnace PEO-401 (ATV Thermal Processing, Vaterstetten, Germany) in inert atmosphere (Ultra-pure nitrogen). The samples were positioned between "dummy" silicon wafers as it shown in the **Figure 3** to create a homogeneous gas flow inside of the tube, even if the number of substrates to pyrolyze vary. The pyrolysis process started with room temperature (25 °C) for 1 hour to create an inert atmosphere by extracting the oxygen using the nitrogen. It was applied a heat ramp of 4.5 °C/min to achieve 300 °C and a second heat ramp (1.67 °C/min) to reach 600 °C **(7)**. Then, it was reached 900 °C by using a heat ramp of 5 °C/min. It was maintained the final temperature for 2 hours and finally, the furnace cooled down at room temperature. The gas flow proportioned during the pyrolysis varied in 1000 mL/min and 5500 mL/min.

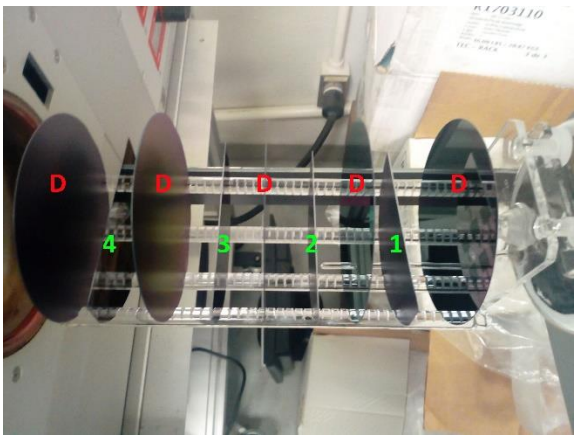

Figure 3. Distribution of "dummy" wafers and samples to pyrolyze. D: Dummy wafer, 1-4: position of sample from 1 (near to the entry of gas) to 4 (near to the outro of gas).

Electrodes characterization

- Preparation of electrodes

The pyrolyzed substrates were numbered from 1 (nearest to the gas inlet) to 4 (farthest to the gas inlet) (**Figure 3**) to check if the spatial position of the substrate affects the electrochemical and surface properties of the electrodes. As well, the electrodes in the same substrate were numbered as it shown in the **Figure 4** to check if the change of position of the electrode respect with height generates variation. The previous steps were performed for all the pyrolyzed substrates in the two gas flows established in the pyrolysis process.

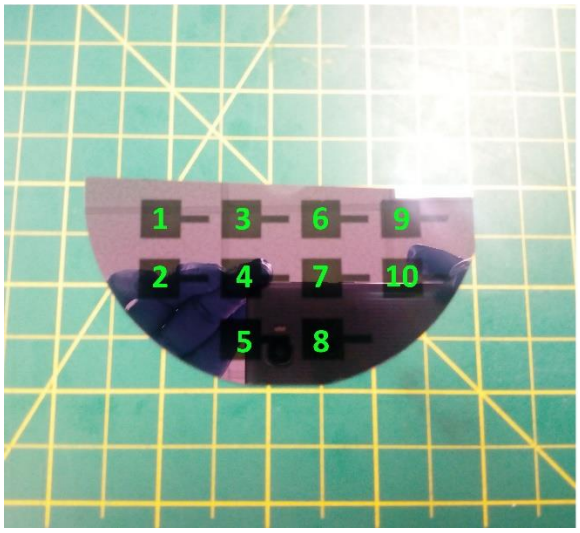

Figure 4. Glassy carbon electrodes obtained from pyrolysis. Numeration of electrodes for further electrochemical studies.

- Surface characterization

Scanning Electron Microscopy (SEM) (Acc. Voltage 10 kV) and optical microscopy will be employed to observe the state of the surface of the electrodes, either for the presence of cracks and fractures or microbubbles because of trapped oxygen **(9,17,18)**. For the non-conductive parts in the sample, a thin gold film will be evaporated on the top to avoid charging **(17,19)**. Cross-sectional images are obtained using SEM to determine the thickness of the carbon structures after pyrolysis **(5)**.

- Chemical environment characterization

Raman spectroscopy is carried out at 532 nm (Ar-ion laser, 10 mW, 1000-1800 cm^{-1}) to check the level of graphitization, or "G/D" ratio, in the pyrolyzed carbon in the two gas flows **(2,5,13)**.

X-Ray photoelectron spectroscopy (XPS) is recorded using a monochromatic Al Kα X-ray source while the measurement chamber is maintained under $<10^{-6}$ Pa vacuum. This pattern was performed in a range of 0 to 1000 eV to determine the levels of oxygen (using the ratio

O_{1s} and C_{1s} peak area) presented in the electrodes while there was variation of gas flow **(2,10,18,19)**.

Attenuated total reflectance-Fourier Transform Infrared spectroscopy (ATR-FTIR) is performed on a solid sample (pyrolyzed carbon structure above of silicon substrate) through a diamond ATR crystal (500-4000 cm^{-1}). This method is used to investigate the conversion of the photoresist to glassy carbon was successful considering that the gas flow was modified at 1000 mL/min and 5500 mL/min **(18,20,21)**.

- Electrochemical characterization

The electrochemical characterization was performed on the pyrolyzed carbon electrodes using cyclic voltammetry (CV) and Electrochemical Impedance Spectroscopy (EIS). The measurements were performed using a potensiostat Chi Instruments 7xx. CV and EIS measurements were acquired using 300 µL 10 mM ferri-ferrocyanide $[Fe(CN)_6]^{4-}/[Fe(CN)_6]^{3-}$ in potassium chloride (KCl).

CV was measured using a scan rate of 100 mV/s from -600 to 600 mV with a three-electrode configuration (working: GCE, counter: platinum, reference: AgCl). CV was employed to assess the electrochemical kinetics of the surface towards oxidation and reduction reactions of molecular species. These properties are evaluated using the Nicholson method, which consists of recording the anodic/cathodic peak separation in a specific scan speed **(22)**. For the case of glassy-like carbon electrodes, the difference of peak potentials must be around 59 mV (Value preestablished for redox reaction of $Fe(CN)_6^{3-/4-}$).

EIS was measured using a two electrodes configuration (WE and CE) acquiring data in the frequency range of 0.1-10^6 Hz with a sinusoidal signal of 10 mV (10 acquisitions points per decade). EIS is used to know the resistance that the electrodes present due to the material and the measurement setup, as well as the presence of capacitance in a quantified way.

Expected Results

Surface characterization

Figure 5a displays a SEM image with a frontal view of the pyrolyzed structure. If the change of gas flow to a lower value can affect the sample in a physical way, it would be the apparition of cracks or fractures by overstress. Although the fractures are related to the adhesion of the SU-8 to the substrate prior to the pyrolysis, the disbalanced thermal stress is the final factor. As well, the existence of a non-homogenous flow through the Quartz tube can generate the thermal stress (related to a temperature gradient existence), being the position of the substrate crucial during the pyrolysis.

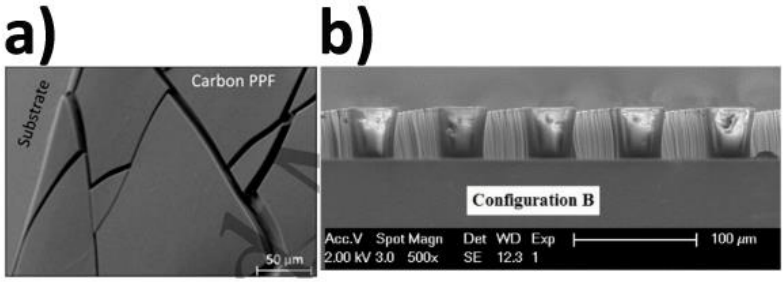

Figure 5. a) SEM image in superior view showing fractures on the carbon structure **(7)**. b) Cross-sectional SEM image used to estimate thickness of pyrolyzed structure **(23).**

Figure 5b displays a cross-sectional SEM image of the pyrolyzed structure. According with Singh et al. **(9)**, Lyon et al. **(16)** and Natu et al. **(14)**, the shrinkage effect in the carbon structures (outgassing of non-carbon material) is related to the final temperature during the pyrolysis and the type of gas used for the atmosphere; the gas flow should not affect this effect. It is expected to obtain a homogenous thickness in the samples either for 5500 mL/min and 1000 mL/min.

Chemical environment characterization

Figure 6 shows a Raman spectra comparison of multiple samples done by Pilloni et al. **(7)**. It is expected to obtain not only the characteristic G-band (graphite, C-C vibrational mode, 1590 cm^{-1}) and D-band (amorphous, Disorder, 1330 cm^{-1}) but a low D/G ratio **(5,6)**. Kakunuri et al. **(13)** concluded that the increase of the final temperature in the pyrolysis can decrease the D/G ratio, which is related to the capacity of conductivity of the material. If the D/G ratio of multiple samples in the gas flow 5500 mL/min and 1000 mL/min does not vary, we could conclude that the gas flow does not affect the graphitization of the glassy carbon electrodes by the uniformity of temperature in all the furnace.

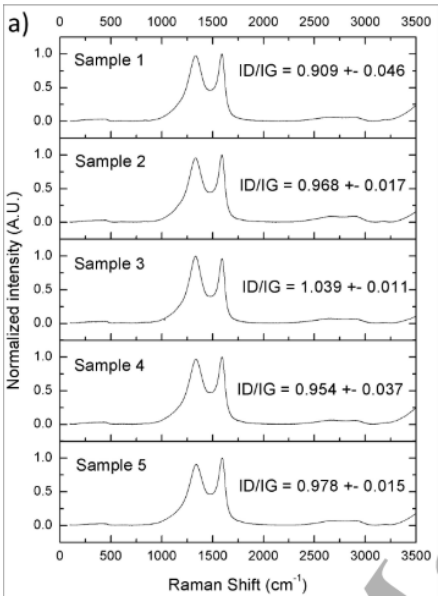

Figure 6. Raman spectra of different samples measuring the graphitization ratio between D and G band **(7).**

The XPS pattern shown in the **Figure 7** is the typical pattern to obtain from the glass-like carbon structure. The peaks that appears after applying pyrolysis are carbon (284.6 eV, related to C=C) and oxygen (531 eV). It is important to check that it was successful the outgassing in the material, because in the case that it was not inert enough the atmosphere (by a low gas flow) it would appear nitrogen or higher oxygen peak **(19)**. If the O/C ratio obtained from all the samples in the two gas flows does not present a significant difference, it is possible to conclude that the gas flow does not affect the inert atmosphere during the pre-carbonization step.

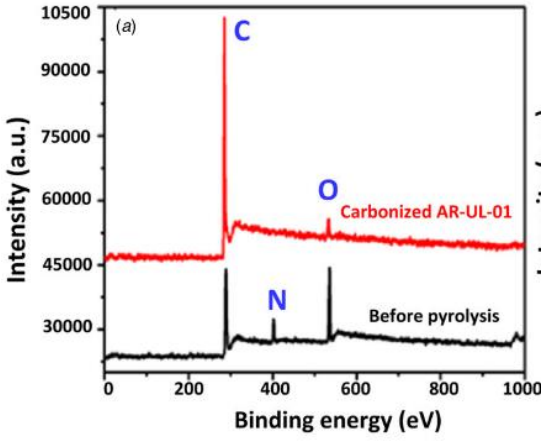

Figure 7. XPS pattern comparing the chemical composition before and after pyrolysis **(19)**

The FTIR spectra is displayed in the **Figure 8**. According with Jin et al. **(20)**, below of 700 °C the photoresist film presents the next peaks: 1250 cm^{-1} (C-O-C stretch), 1500 cm^{-1}

(C-C stretch aromatic rings) and 3500 cm^{-1} (hydroxyl stretch). However, above of 700 °C the spectrum does not present any significant peak because the material was able of completing the carbonization (infrared inactive). Nam et al. **(18)** showed that is possible to observe a small peak in 1503 cm^{-1}, related to the carbonization of the material. We are expecting to obtain smooth line in the spectra of the samples, demonstrating the glassy carbon electrodes were successful to eject the rest of the oxygen and hydrogen of the composition, just possible if the inert atmosphere was not compromise by a low gas flow (1000 mL/min). The XPS pattern and FTIR spectrum are complementary to determine the purity of the pyrolyzed structures, without a compromising noncarbon material on it.

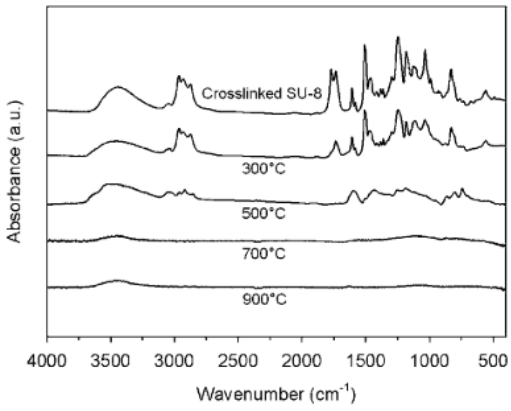

Figure 8. FTIR spectra showing the disappearance of peaks before of pyrolysis to a 900 °C carbon structure, being the full carbonization of the material **(20)**

Electrochemical characterization

The **Figure 9** shows examples of CVs where each one varies depending of the final temperature used during the pyrolysis. Singh et al. **(9)** and Mardegan et al. **(6)** concluded that the reduction of the difference of potentials (ΔE) between the anodic and cathodic peaks as well as the increase of current peak (Ip), are signals of a high conductivity of the glassy carbon electrodes. Hassan et al. **(5)** showed that the dwell time and heating rate do not represent relation with the previous parameters. We expected that the samples show similar ΔE independent of the position of the electrodes in the Quartz tube during the pyrolysis. The previous statement can demonstrate that the change of gas flow does not affect the electrochemical behavior.

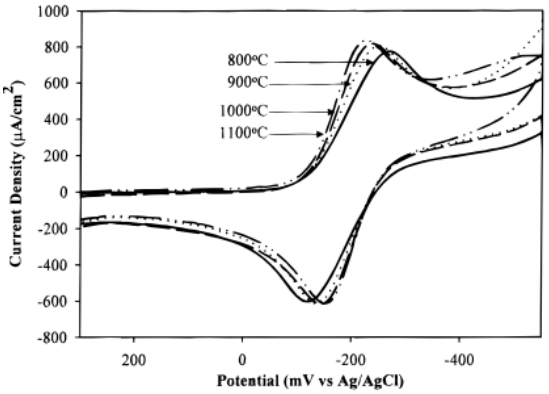

Figure 9. CV curves displaying the decrease of difference of potential by increasing the final temperature during pyrolysis, being a better electrochemical performance **(10)**

The **Figure 10** shows examples of EIS curves where each one changes to lower value if the dwell time increases. According with Hassan et al. **(5)**, it is expected that the diameter of the big semi-circle represents the charge transfer resistance (resistance generated by the redox reaction near of the surface electrode) and the intersection of the linear part in the X axis is the solution and electrode resistance. We expected to obtain similar resistance in the samples where the samples were taken from different parts of the Quartz furnace. It is possible to conclude that both the CVs and EIS results are complementary, where our samples can be enhanced their electrochemical properties in low gas flow.

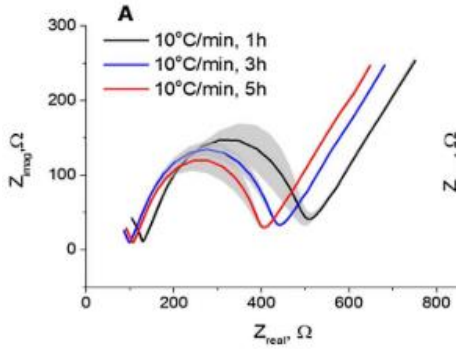

Figure 10. EIS curves obtained by varying the heat rates during the pyrolysis **(5)**

Summary about the characterization methods

The use of characterization techniques on this project was useful to visualize and understand the flaws during the pyrolysis, either the manipulation of the material and gas and the spatial localization of the substrates on the Quartz tube. The SEM images are useful to know the state of the carbon structures after the pyrolysis, checking if there are fractures or crack because of overstress by heat. The chemical composition characterization is used for two purposes: 1) To confirm that the carbon structure obtained from SU-8 has similar properties of commercial glassy carbon (using especially Raman and XPS) and 2) To quantify the fabrication quality in terms of the successful outgassing and conductivity after the

pyrolysis in different samples along the Quartz tube. The electrochemical characterization is used to evaluate the electrochemical performance of the carbon electrodes as a redox reaction sensor, while checking that the spatial localization during the pyrolysis did not affect these properties. It was omitted techniques such as thermal ones and X-Ray Diffraction (XRD); the first ones because the loss of mass during the pyrolysis is well known and do not provide contribution for the purpose of the project. XRD has been explored for other authors only for confirmation intentions to compare the structures obtained from pyrolyzed SU-8 with glassy carbon. For this project, it is assumed that our carbon structures are comparable to glassy carbon, being confirmed this using Raman, XPS and FTIR.

Conclusion

This project will help not only to reduce materials costs (gas tank and loss of material by failed fabrication) but to obtain electrodes with good electrochemical properties. After the optimization of gas flow and spatial localization of substrates in pyrolysis, it will be possible to see the possibilities of creating protocols for electrodes fabrication that include either nanoparticles or surface functionalization.

References

1. Aeinehvand MM, Fatimah I, Al-Faqheri W, Joseph K, Madou MJ. Recent advances in the development of micropumps, microvalves and micromixers and the integration of carbon electrodes on centrifugal microfluidic platforms. Int J Nanotechnol. 2018;15(1/2/3):53–68.
2. Peltola E, Heikkinen JJ, Sovanto K, Sainio S, Aarva A, Franssila S, et al. SU-8 based pyrolytic carbon for the electrochemical detection of dopamine. J Mater Chem B. 2017;5(45):9033–44.
3. Kim TH, Abi-Samra K, Sunkara V, Park DK, Amasia M, Kim N, et al. Flow-enhanced electrochemical immunosensors on centrifugal microfluidic platforms. Lab Chip. 2013;13(18):3747–54.
4. Martinez-Duarte R, Gorkin RA, Abi-Samra K, Madou MJ. The integration of 3D carbon-electrode dielectrophoresis on a CD-like centrifugal microfluidic platform. Lab Chip. 2010;10(8):1030–43.
5. Hassan YM, Caviglia C, Hemanth S, Mackenzie DMA, Alstrøm TS, Petersen DH, et al. High temperature SU-8 pyrolysis for fabrication of carbon electrodes. J Anal Appl Pyrolysis [Internet]. 2017;125(November 2016):91–9. Available from: http://dx.doi.org/10.1016/j.jaap.2017.04.015
6. Mardegan A, Kamath R, Sharma S, Scopece P, Ugo P, Madou M. Optimization of Carbon Electrodes Derived from Epoxy-based Photoresist. J Electrochem Soc [Internet]. 2013;160(8):B132–7. Available from: http://jes.ecsdl.org/lookup/doi/10.1149/2.107308jes
7. Pilloni O, Madou M, Mendoza D, Muhl S, Oropeza-Ramos L. Methodology and fabrication of adherent and crack-free SU-8 Photoresist-derived Carbon MEMS on Fused Silica Transparent Substrates. J Micromechanics Microengineering. 2019;29.
8. Martinez-Duarte R. SU-8 photolithography as a toolbox for carbon MEMS. Micromachines. 2014;5(3):766–82.
9. Singh A, Jayaram J, Madou M, Akbar S. Pyrolysis of Negative Photoresists to Fabricate Carbon Structures for Microelectromechanical Systems and Electrochemical Applications. J

Electrochem Soc. 2002;149(3):E78.
10. Ranganathan S, McCreery R, Majji SM, Madou M. Photoresist-Derived Carbon for Microelectromechanical Systems and Electrochemical Applications. J Electrochem Soc. 2002;147(1):277.
11. Wang C, Jia G, Taherabadi LH, Madou MJ. A novel method for the fabrication of high-aspect ratio C-MEMS structures. J Microelectromechanical Syst. 2005;14(2):348–58.
12. Kakunuri M, Sharma CS. Effect of Current Collector and Pyrolysis Temperature on the Electrochemical Performance of Photoresist Derived Carbon Films. ECS J Solid State Sci Technol. 2017;6(6):M3001–6.
13. Kakunuri M, Sharma CS. Effect of Pyrolysis Temperature on Electrochemical Performance of SU-8 Photoresist Derived Carbon Films. ECS J Solid State Sci Technol. 2016;6(6):M3001–6.
14. Natu R, Islam M, Gilmore J, Martinez-Duarte R. Shrinkage of SU-8 microstructures during carbonization. J Anal Appl Pyrolysis [Internet]. 2018;131(January):17–27. Available from: https://doi.org/10.1016/j.jaap.2018.02.015
15. Tang Z, Shi T, Gong J, Nie L, Liu S. An optimized process for fabrication of high-aspect-ratio photoresist-derived carbon microelectrode array on silicon substrate. Thin Solid Films [Internet]. 2010;518(10):2701–6. Available from: http://dx.doi.org/10.1016/j.tsf.2009.09.048
16. Lyons AM, Hale LP, Wilkins CW. Photodefinable carbon films: Control of image quality. J Vac Sci Technol B Microelectron Process Phenom [Internet]. 1985 Jan 1;3(1):447–52. Available from: https://avs.scitation.org/doi/abs/10.1116/1.583284
17. Sharma CS, Sharma A, Madou M. Multiscale carbon structures fabricated by direct micropatterning of electrospun mats of SU-8 photoresist nanofibers. Langmuir. 2010;26(4):2218–22.
18. Nam H-G, Jung J-M, Hwang I-T, Shin J, Jung C-H, Choi J-H. Preparation of photoresist-derived carbon micropatterns by proton ion beam lithography and pyrolysis. Carbon Lett. 2017;24(1):55–61.
19. Penmatsa V, Kawarada H, Wang C. Fabrication of carbon nanostructures using photo-nanoimprint lithography and pyrolysis. J Micromechanics Microengineering. 2012;22(4).
20. Jin WM, Moon JH. Supported pyrolysis for lithographically defined 3D carbon microstructures. J Mater Chem. 2011;21(38):14456–60.
21. Vomero M, Van Niekerk P, Nguyen V, Gong N, Hirabayashi M, Cinopri A, et al. A novel pattern transfer technique for mounting glassy carbon microelectrodes on polymeric flexible substrates. J Micromechanics Microengineering [Internet]. 2016;26(2):25018. Available from: http://dx.doi.org/10.1088/0960-1317/26/2/025018
22. Elgrishi N, Rountree KJ, McCarthy BD, Rountree ES, Eisenhart TT, Dempsey JL. A Practical Beginner's Guide to Cyclic Voltammetry. J Chem Educ. 2018;95(2):197–206.
23. Ginestra PS, Madou M, Ceretti E. Production of carbonized micro-patterns by photolithography and pyrolysis. Precis Eng [Internet]. 2019;55(June 2018):137–43. Available from: https://doi.org/10.1016/j.precisioneng.2018.08.019